NASA TN D-1219

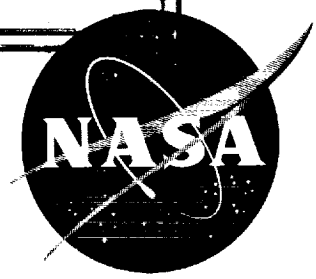

TECHNICAL NOTE

D-1219

COMPARATIVE MEASUREMENTS OF SINGLY AND DOUBLY IONIZED MERCURY PRODUCED BY ELECTRON-BOMBARDMENT ION ENGINE

By Nelson L. Milder

Lewis Research Center
Cleveland, Ohio

NATIONAL AERONAUTICS AND SPACE ADMINISTRATION
WASHINGTON
July 1962

NATIONAL AERONAUTICS AND SPACE ADMINISTRATION

TECHNICAL NOTE D-1219

COMPARATIVE MEASUREMENTS OF SINGLY AND DOUBLY IONIZED MERCURY PRODUCED BY ELECTRON-BOMBARDMENT ION ENGINE

By Nelson L. Milder

SUMMARY

A mass spectrometer employing a fixed magnetic field was used to analyze the ion-beam exhaust of an electron-bombardment ion engine. The beam was studied at several steady-state operating conditions. The ion-chamber potential difference was varied between 20 and 100 volts for net accelerating potentials ranging from 900 to 4900 volts.

From the observed data, the relative current densities of doubly and singly ionized mercury were estimated. The fraction of the total beam current due to doubly charged mercury varied from less than 0.05 at low ion-chamber potential differences to over 0.3 at the high potential differences. The presence of these doubly charged mercury ions in the beam reduced the calculated thrust by less than 10 percent at an ion-chamber potential difference of 100 volts and by only about 4 percent at a potential difference of 50 volts.

INTRODUCTION

In its present stage of development, the electron-bombardment ion-rocket engine appears to employ an efficient method for creating and accelerating ions to obtain thrust (refs. 1 to 3). Theoretical considerations indicate that the process by which ions are created in such an engine may result in the formation of differently charged ions; for example, the propellant generally used is mercury, which may form singly, doubly, or triply charged ions (Hg^{+}, Hg^{++}, and Hg^{+++}, respectively) in the range of bombardment electron energies of interest (up to 100 ev). Since the occurrence of doubly and triply ionized mercury in any appreciable quantity is undesirable on the basis of overall engine performance, there is a need for ascertaining the degree to which such ions are produced. Accordingly, a series of tests was made using a simple magnetic mass spectrometer to determine the approximate fractions of the ion beam attributable to the various ionic species. An estimate of the effect on overall engine performance due to the production of doubly ionized mercury is also presented.

SYMBOLS

B	magnetic field strength, gauss
C	hot-wire calorimeter sensitivity constant, amp^2/cm^2
d	ion displacement from initial trajectory, cm
E	calorimeter output voltage
e	electronic charge, 1.6×10^{-19} coulomb
j_n	generalized current density, amp/cm^2
j_T	current density of ion beam, amp/cm^2
j_+	current density of Hg^+, amp/cm^2
j_{++}	current density of Hg^{++}, amp/cm^2
l	length of magnetic field region, cm
m	ion mass, g
m_-	electron mass, g
n_0	density of neutrals, cm^{-3}
n_+	density of Hg^+, cm^{-3}
n_{++}	density of Hg^{++}, cm^{-3}
n_-	density of electrons, cm^{-3}
q	ionic charge, coulombs
R	radius of ion trajectory in magnetic field, cm
r	radius of arc traversed by detector probe, cm
T/A	thrust per unit area, $dynes/cm^2$
t	time, sec
V_A	accelerator voltage
V_I	ion net accelerating voltage

ΔV_I ion-chamber potential difference between anode and cathode, v

v ion velocity, cm/sec

v_- electron velocity, cm/sec

$\bar{v}_-$ mean electron velocity, cm/sec

Z number of electronic charges

α fraction of total ion beam due to Hg^{++}

$\sigma_{0,1}$ electron-atom single ionization cross section, cm^2

$\sigma_{0,2}$ electron-atom double ionization cross section, cm^2

$\sigma_{1,2}$ electron-ion double ionization cross section, cm^2

APPARATUS

Vacuum Facility

The experiment was performed in one of the electric-rocket vacuum test facilities at the Lewis Research Center. A cutaway sketch of the vacuum tank with the engine and spectrometer installed is shown in figure 1. The spectrometer was mounted at two positions, 18 and 42 inches downstream of the engine, and was alined by motor-driven actuators mounted inside the tank. The tank pressure was maintained at about 10^{-6} millimeter of mercury. A more detailed description of the vacuum facility is given in reference 4.

Ion Engine

An electron-bombardment ion-rocket engine was used employing mercury as the propellant. A cutaway drawing of the engine is shown in figure 2(a), and figure 2(b) is a schematic diagram showing the essential components and power supplies. Detailed descriptions of this engine are given in references 2 and 3. High-velocity electrons emitted from a hot filament collide with mercury atoms and ionize some of them. A weak magnetic field (20 to 30 gauss) is provided to increase the electron path length and, hence, the collision probability. The ions that pass through the screen are accelerated rearward to produce an ion beam.

The engine was operated at net accelerating voltages V_I (see fig. 2(b)) ranging from 900 to 4900 volts. Electron energies producing the ions were characterized by the ion-chamber potential difference ΔV_I and ranged from 20 to 100 volts. All tests were made at a propellant utilization efficiency of about 80 percent.

Description of Spectrometer

A simple mass spectrometer (fig. 3) consisting of a constant magnetic field of 400 gauss was used to separate differently charged mercury ions from the total beam. A detailed description of the various components shown in figure 3 follows.

Magnetic field. - The magnetic field was provided by 22 bar magnets, 1 inch in diameter and 2 inches long, mounted between two high-permeability steel plates (figs. 3 and 4). The effective length of the constant field region was about 10 inches with a rectangular opening between plates of about 2 by 6 inches. The field strength was measured with a Hall effect gauss meter and was uniformly 400 gauss to within ±5 gauss between the two steel plates. A copper sheet with a centered 1-inch-diameter hole was attached to the front of the magnet assembly to provide a means for mounting collimating slits of various sizes. The top plate was extended in order to support the detector actuating system as shown in figure 4.

Collimator. - Two coaxially mounted slits separated about 10 inches were used to collimate the ion beam. The relative positions of these slits are shown in figure 3.

Different slit size combinations were tried in order to find a combination that gave a good narrow beam while keeping transmitted power as high as possible. A further discussion of these slit sizes is presented in the Spectrometer Adjustments section.

Detector. - Two hot-wire calorimeters were used to survey the beam upstream and downstream of the magnetic field, so that a comparison between incident and transmitted beam power could be made. The arrangement of the calorimeters is shown in figures 3 and 4. A detailed description and analysis of the hot-wire calorimeter is given in reference 5. Upon striking a small fine wire (0.005-in. diam. by 0.375 in. long), the ion beam heats the wire and changes its resistance. A small constant current through the wire is used to measure this resistance change, which corresponds to the power density in the beam. The high sensitivity of this device proved to be well suited to the experiment, since a very small fraction of the total beam power entered the magnetic field. The hot wires were supported by 1/4-inch-outside-diameter, 0.049-inch-wall tubing. The probe was so mounted as to pivot about an axis coincident with the entrance slit. The mounting enabled surveys to be made over an arc of 30°, which covered the total field gap. The position of the front (upstream) probe relative to the back (downstream) probe was offset, so that interference did not occur. The hot-wire probe traverse was monitored by means of a biased 100,000-ohm potentiometer, such that the variation in the d-c signal produced by one complete turn of the potentiometer corresponded to full-scale traverse of the probe. This d-c signal was fed to the x-axis of an x-y plotter.

The beam signal, as detected by the hot-wire calorimeter, was fed to the y-axis of the recorder through a d-c amplifier set at a gain of about 300. The resulting signal-to-noise ratio varied between 5:1 and about 30:1, depending upon the engine operating conditions.

Housing. - A cylindrical water-cooled copper can approximately 1 foot in diameter by 2 feet long was used to house the spectrometer assembly. A honeycomb shield was placed on the end of the can facing the ion rocket. The first collimating slit was placed in the plane of this shield. A copper plate with a $1\frac{1}{2}$-inch-diameter hole was placed between the front of the can and the magnet assembly in order to isolate the detector actuator and magnet assembly from the beam. The can was water-cooled to provide a constant temperature environment for the detectors.

The magnet was fastened to the inner wall of the can in a fashion amenable to optical alinement of the two collimating slits. The copper housing was so connected to an actuator system mounted to the inner walls of the vacuum tank that small alinement adjustments could be made in two directions transverse to the direction of the beam.

Theory of Spectrometer Operation

The spectrometer used in this investigation employed the well-known action of a $Ze(\vec{v} \times \vec{B})$ force on a charged particle. An ion with velocity v entering a magnetic field B along a trajectory perpendicular to the field is deflected in a circular path of radius R according to the relation

$$m \frac{v^2}{R} = BZev \tag{1}$$

The initial velocity of the ion is that obtained by so accelerating it through a potential difference V_I (see fig. 3) as to impart an energy given by

$$\frac{1}{2} mv^2 = ZeV_I \tag{2}$$

Therefore,

$$v = \left(\frac{2ZeV_I}{m}\right)^{1/2} \tag{3}$$

From equations (1) to (3), for a constant magnetic field strength, the radius of curvature R can be written as

$$R = \frac{1}{B}\left(\frac{2mV_I}{Ze}\right)^{1/2} \tag{4}$$

The ion trajectory is shown in the following sketch:

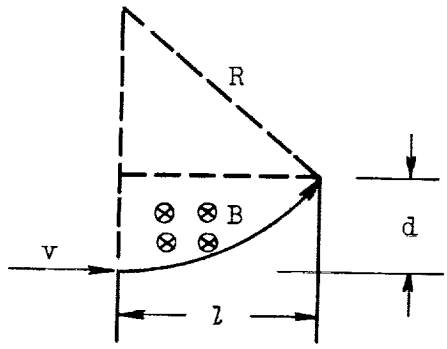

The perpendicular distance d between the initial ion trajectory and the position of the ion upon leaving the magnetic field is related to R and the effective field length l by the equation

$$d = R\left[1 - \left(1 - \frac{l^2}{R^2}\right)^{1/2}\right] \tag{5}$$

Because of the manner in which the hot-wire probes were mounted and actuated, the ion beam was traversed along a small segment of circular arc. The radius r of this circle was large (~1 ft) and $l \simeq r$, however, so that to a good approximation the deflected beam position on this arc corresponded to d.

Theory of Detector Operation

The theory of operation of the hot-wire calorimeter is described thoroughly in reference 5 and will not be treated in detail herein. Only one of the basic relations of the wire operation need be presented. With constant current J through the wire, the output voltage E is related to the local ion current density j by the relation

$$\left[\frac{\Delta(jV_I)}{\Delta E}\right]_{J=\text{const}} = \frac{C}{J}, \frac{w}{(cm^2)(v)} \tag{6}$$

where C is the sensitivity constant and ΔE is the voltage drop across the wire. From this relation current density j_n can be expressed in terms of measurable parameters, since

$$j_n = \frac{C}{J}\frac{SA}{V_I} \tag{7}$$

where S is the scale factor on the plotter and A is the area under the recorded curves. This relation shows that the ratio between current densities of the different ionic species at a given acceleration voltage and ion-chamber potential difference is equal to the ratio of the areas corresponding to these species.

Spectrometer Adjustments

In order to obtain conditions of optimum transmission and resolution, the following three variables were utilized: (1) the distance between the spectrometer and the engine, (2) the alinement of the spectrometer with the engine so that the ion beam was incident on the spectrometer slits, and (3) the selection of collimating slit sizes. The manner in which these three parameters were varied is described subsequently.

Because of mechanical and spatial limitations, the spectrometer was mounted at only two fixed distances from the engine. The experiment was performed at each of the two positions. The first experiment was performed for an engine-spectrometer separation of about 42 inches; whereas the second experiment was performed at a separation of about 18 inches.

The actuator system attached to the spectrometer housing was used to aline the device with the engine without opening the vacuum facility. Thus the proper alinement could be maintained by adjusting the spectrometer while the engine was in operation. Variation of the spectrometer alinement indicated that the maximum transmission did not coincide with visual alinement, presumably because of accelerator anomalies or space-charge effects in the beam.

The fraction of the beam transmitted, as measured by the ratio of the beam power passing through the magnetic field to the power passing through the first slit (fig. 3), was approximately constant at 0.02 for both spectrometer positions. Thus the results proved to be insensitive to spectrometer position over the range of operating conditions investigated.

In order to optimize transmission and resolution simultaneously, collimating slits of various sizes were tested. The slits were about 19 millimeters in length and varied in width. Trial and error showed that the best results were obtained for a front slit width of 3 millimeters and a back slit width of 2 millimeters.

RESULTS AND DISCUSSION

Resolution

The experiment revealed the existence of only two ionic species in the range of engine operation employed (fig. 5). It will be shown later that the observed peaks can be identified with Hg^{+} and Hg^{++}. The resolution (i.e., the ability to separate the different ionic species) decreases with increasing accelerating voltage. This sharp dependence of resolution on accelerating voltage is to be expected, since the spectrometer used only a $\vec{v} \times \vec{B}$ field with constant $\vec{B}$ (rather than the generally used $\vec{E} \times \vec{B}$ field) to separate the ions. The experiment was not designed for optimum spectroscopic analysis of an ion beam, however, and the instrument did serve the purpose for which it was intended.

The line widths at half maximum intensity remained fairly constant and independent of engine operating potentials (fig. 5). This fact would seem to imply that no appreciable velocity distribution (resulting from grid aperture effects, distributions in mass, etc.) existed over the portion of the ion beam passing through the spectrometer, since marked variation in line widths with varying accelerating potentials could be expected. The observed line widths can be attributed to an energy distribution characteristic of the geometrical arrangement of the spectrometer collimating slits and the hot-wire calorimeter.

Identification of Peaks

The theoretical dependence of the displacement d on the radius of curvature R of the ion trajectory in a magnetic field (and thus on the accelerating voltage V_I) enables calculation of the dependence of the separation between beam intensity peaks Δd on accelerating voltage.

This dependence is shown in figure 6 for the separation between Hg^{+} and Hg^{++} in a field of 400 gauss. The data points represent observed separations. Of course, the error in measuring these separations increased with decreasing resolution (and, hence, increasing voltage). At an ion net accelerating voltage of 900 volts, the probable error in measurement was about 3 percent; whereas, at 4000 volts, the error was about 20 percent. The general trend of the data indicates fairly conclusively that the two observed peaks corresponded to singly and doubly ionized mercury.

The relative peak separation Δd rather than the peak displacement from the spectrometer axis was used to interpret the data. Comparison of the observed peak positions with the calibrated probe traverse indicated displacements greater than those expected from theoretical considerations. An attempt to identify the observed data with masses

other than mercury proved futile. Subsequent investigation which indicated that the ion beam axis was not coincident with the engine spectrometer axis accounted for the apparent discrepancy. The peak-to-peak separation, however, would not be affected by this phenomenon, and thus could be obtained directly from the data.

The presence of Hg^{+++} was not observed at any of the operating conditions employed in this experiment; however, it should be pointed out that this does not rule out the possibility for the occurrence of Hg^{+++} at these conditions. The amount of Hg^{+++} produced should probably be small and well within the noise level of the detecting system.

Secondary Ionization Measurements

The main process by which ions are produced in an electron-bombardment engine is electron-atom collisions. Electrons with energies greater than about 10 electron volts may collide with mercury atoms to produce Hg^{+}; while electrons with energies greater than about 30 electron volts may produce Hg^{++} ions. Cross sections for these ionizing collisions are presented in references 2, 6, and 7 as a function of electron energy. The ionization process can be described in terms of ion production ratio (ions/(cm^3)(sec)) as follows:

$$\frac{dn_{++}}{dt} = \sigma_{0,2} n_0 n_- \bar{v}_- \tag{8a}$$

$$\frac{dn_{+}}{dt} = \sigma_{0,1} n_0 n_- \bar{v}_- \tag{8b}$$

In terms of current densities,

$$\frac{j_{++}}{j_{+}} = 2 \frac{\sigma_{0,2}}{\sigma_{0,1}} \tag{9}$$

The factor 2 occurs because of the two electronic charges of a doubly ionized atom. A graph of equation (9) is represented by the solid curve in figure 7. Note that relations (8) are valid for monoenergetic ionizing electrons. In the case of the electron-bombardment engine, however, the ionizing electrons emitted at the ion-chamber voltage ΔV_I are not monoenergetic, and a more precise relation would have the form

$$\frac{dn_{++}}{dt} = \int_{v_-=0}^{v_-=(2e\ \Delta V_I/m_-)^{1/2}} \sigma_{0,2}(v_-) n_0 n_-\ dv_- \tag{10}$$

Since the curve in figure 7 was determined from cross sections corresponding to monoenergetic electrons, it is probably higher than one that would have been obtained with an integrated expression such as equation (10).

In addition to the electron-atom collisions, there may occur collisions of a second kind, namely, electron-ion collisions, which would have a tendency to increase the Hg^{++} yield. The magnitude of the second type of ion-producing process can be estimated by including in equations (8) an additional term as follows:

$$\frac{dn_{++}}{dt} = \sigma_{0,2} n_0 n_- \bar{v}_- + \sigma_{1,2} n_+ n_- \bar{v}_- \tag{11a}$$

$$\frac{dn_{+}}{dt} = \sigma_{0,1} n_0 n_- \bar{v}_- - \sigma_{1,2} n_+ n_- \bar{v}_- \tag{11b}$$

Again, in terms of current densities, in this case,

$$\frac{j_{++}}{j_+} = 2\left(\frac{\sigma_{0,2}}{\sigma_{0,1} - \frac{n_+}{n_0}\sigma_{1,2}} + \frac{n_+}{n_0}\frac{\sigma_{1,2}}{\sigma_{0,1} - \frac{n_+}{n_0}\sigma_{1,2}}\right) \tag{12}$$

In making the preceding estimations, charge exchange processes in the beam have not been considered. Presumably, the ionized products of these reactions would not contribute substantially to the ion beam current density as measured by the hot-wire calorimeters, since they would be low-velocity ions, that is, of the order of neutral velocity.

The data of figure 7 indicate values of j_{++}/j_+ greater than those predicted from equation (9). If this increase is attributed to electron-ion collisions, it should be possible to estimate the cross section for this process from equation (12). Unfortunately the ion and neutral densities are not known with sufficient accuracy to justify a calculation of $\sigma_{1,2}$ at this time.

Effect on Engine Performance

As mentioned earlier in the report, the presence of Hg^{++} in the ion beam is undesirable on the basis of overall engine efficiency. Ideally, an ion beam composed of 100 percent Hg^{+} producing a required thrust is desirable. In reference 9 it is shown that the thrust per unit area can be represented by an equation of the form

$$\frac{T}{A} = 2^{1/2} j\left(\frac{m}{q}\right)^{1/2} V_I^{1/2} \tag{13}$$

where j is the current density. In this section the effect of Hg^{++} on thrust calculations is estimated from the measured values of current density ratio j_{++}/j_T. This ratio, determined from graphic traces similar to those shown in figure 5, was found to vary between approximately 0.05 at an ion-chamber potential difference of 30 volts and 0.3 at 100 volts.

The actual thrust per unit area produced by an electron-bombardment engine can be written

$$\frac{T_{actual}}{A} = \left[j_+ \left(\frac{m}{q}\right)_+^{1/2} + j_{++} \left(\frac{m}{q}\right)_{++}^{1/2} \right] 2^{1/2} V_I^{1/2} \tag{14}$$

which can be rewritten as

$$\frac{T_{actual}}{A} = \left(j_+ + 2^{-1/2} j_{++} \right) \left(\frac{m}{q}\right)_+^{1/2} 2^{1/2} V_I^{1/2} \tag{15}$$

The factor $2^{-1/2}$ occurs because of the two charges associated with the doubly charged ion.

The ideal thrust that would have been obtained if only singly charged mercury ions were in the beam is simply

$$\frac{T_{ideal}}{A} = j_T \left(\frac{m}{q}\right)_+ 2^{1/2} V_I^{1/2} \tag{16}$$

with j_T the total current density in the beam. The ratio of actual to ideal thrust is, then,

$$\frac{T_{actual}}{T_{ideal}} = \frac{j_+ + 2^{-1/2} j_{++}}{j_T} = \frac{j_+}{j_T} + 2^{-1/2} \frac{j_{++}}{j_T} \tag{17}$$

If the fraction of j_T due to Hg^{++} is denoted as α, then

$$\left.\begin{aligned} j_{++} &= \alpha j_T \\ j_+ &= (1 - \alpha) j_T \end{aligned}\right\} \tag{18}$$

Substituting equations (18) into (17) gives the relation

$$\frac{T_{actual}}{T_{ideal}} \cong 1 - 0.3\,\alpha \tag{19}$$

Estimates of thrust reduction due to doubly charged ions can be made from equation (19). For electrons emitted with 100 electron volts, the thrust reduction would be about 9 percent. At a more realistic operating condition (ΔV_I = 50 v) the thrust reduction would be about 4 percent. If the accelerating voltage were increased sufficiently to compensate for the drop in thrust, the accelerating power would have to be increased about 8 percent at ΔV_I = 50 volts, and about 21 percent at ΔV_I = 100 volts. It should thus be apparent that the ion-chamber potential difference should be kept at 50 volts or less if large losses due to double ionization are to be avoided. However, other factors (e.g., cathode emission characteristics, engine stability, etc.) must also be considered when the optimum value of chamber potential difference is established. At present, the best overall engine performance is obtained for ΔV_I of 50 volts.

SUMMARY OF RESULTS

Comparative measurements of singly and doubly ionized mercury produced by an electron-bombardment ion engine were made in order to obtain in a simple and expedient manner some indication of the degree to which multicharged ions influence the overall performance of an electron-bombardment ion engine.

The experiment provided good order-of-magnitude measurements. Limitations on data reliability were introduced mainly as a result of the low resolution of the spectrometer. Engine instability at some of the off-design operating conditions also limited the range of available data to regions of stable operation. The data indicated that the fraction of the total ion beam current attributable to doubly charged mercury ions varied from about 0.05 at an ion-chamber potential difference of 30 volts to about 0.3 at 100 volts. The presence of these ions in the beam had only a slight effect on engine thrust and reduced the calculated value by less than 10 percent at an ion-chamber potential difference of 100 volts and by about 4 percent at 50 volts.

Lewis Research Center
National Aeronautics and Space Administration
Cleveland, Ohio, February 16, 1962

REFERENCES

1. Mickelsen, William R.: Electric Propulsion for Space Flight. Aerospace Eng., vol. 19, no. 11, Nov. 1960, pp. 6-11; 36.

2. Kaufman, Harold R.: An Ion Rocket with an Electron-Bombardment Ion Source. NASA TN D-585, 1961.

3. Kaufman, H. R., and Reader, P.: Experimental Performance of an Ion Rocket Employing Electron Bombardment Ion Source. Preprint 1374-60, Am. Rocket Soc., Inc., 1960.

4. Keller, Thomas A.: NASA Electric Rocket Test Facilities. Paper R-25, Nat. Vacuum Symposium, Oct. 1960.

5. Baldwin, Lionel V., and Sandborn, Virgil A.: Hot-Wire Calorimetry: Theory and Application to Ion Rocket Research. NASA TR R-98, 1961.

6. Massey, H. S. W., and Burhop, E. H. S.: Electronic and Ionic Impact Phenomena. Clarendon Press (Oxford), 1956.

7. Brode, Robert B.: The Quantitative Study of the Collisions of Electrons with Atoms. Rev. Modern Phys., vol. 5, no. 4, Oct. 1933, pp. 257-279.

8. Guthrie, A., and Wakerling, R. K., eds.: The Characteristics of Electrical Discharges in Magnetic Fields. McGraw-Hill Book Co., Inc., 1949.

9. Kaufman, Harold R.: One-Dimensional Analysis of Ion Rockets. NASA TN D-261, 1960.

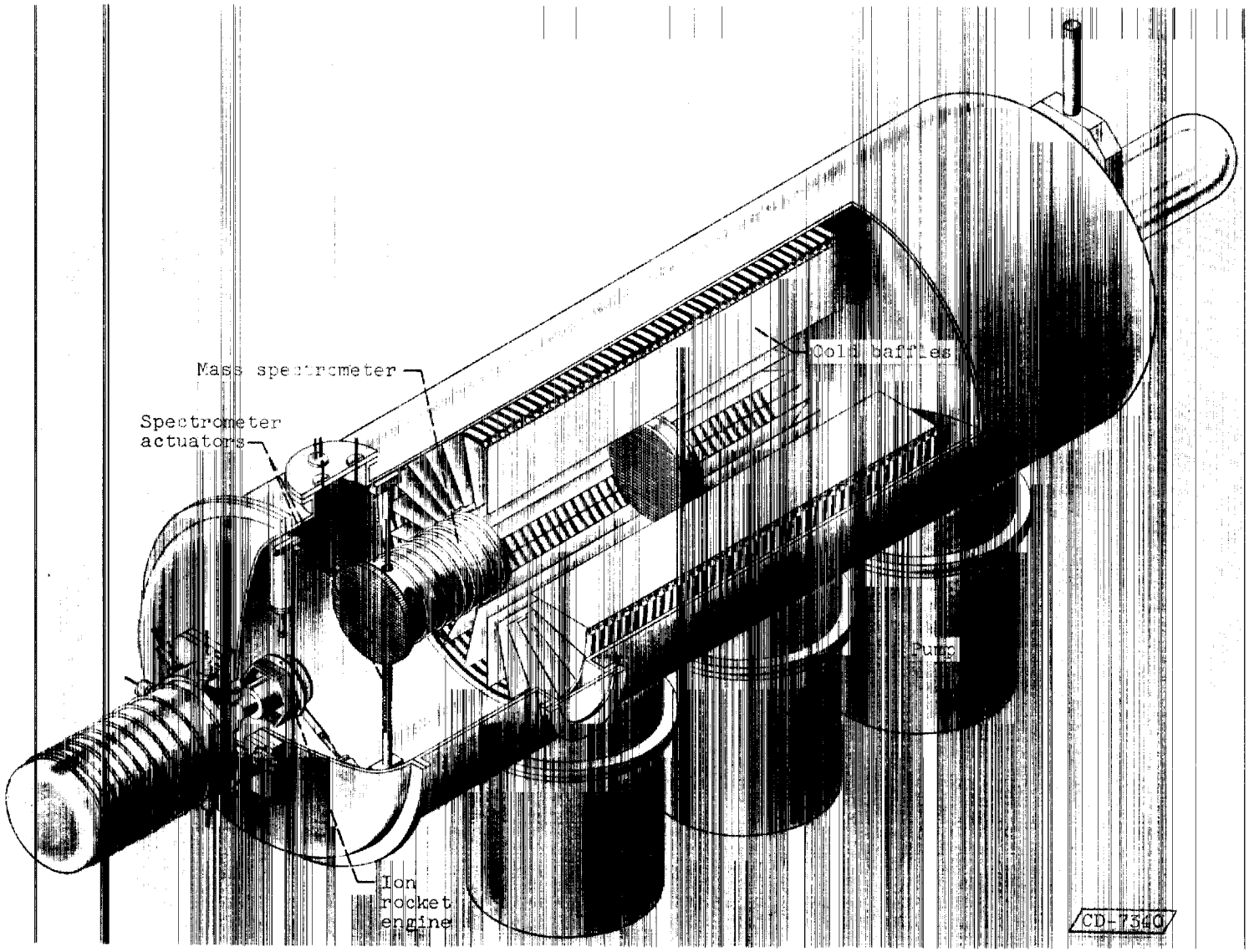

Figure 1. - Engine and spectrometer positions in vacuum facility.

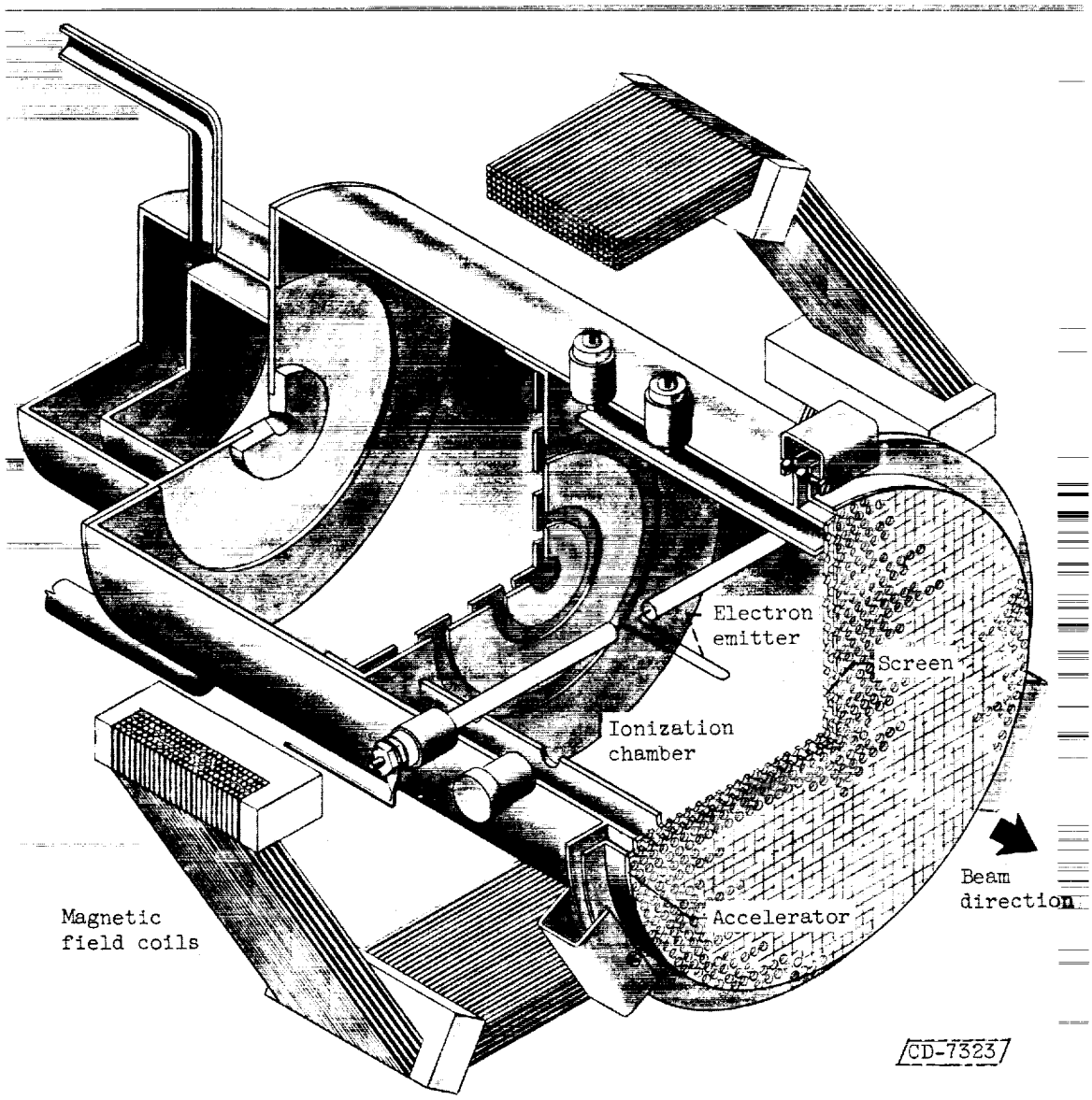

(a) Cutaway drawing.

Figure 2. - Electron-bombardment ion-rocket engine.

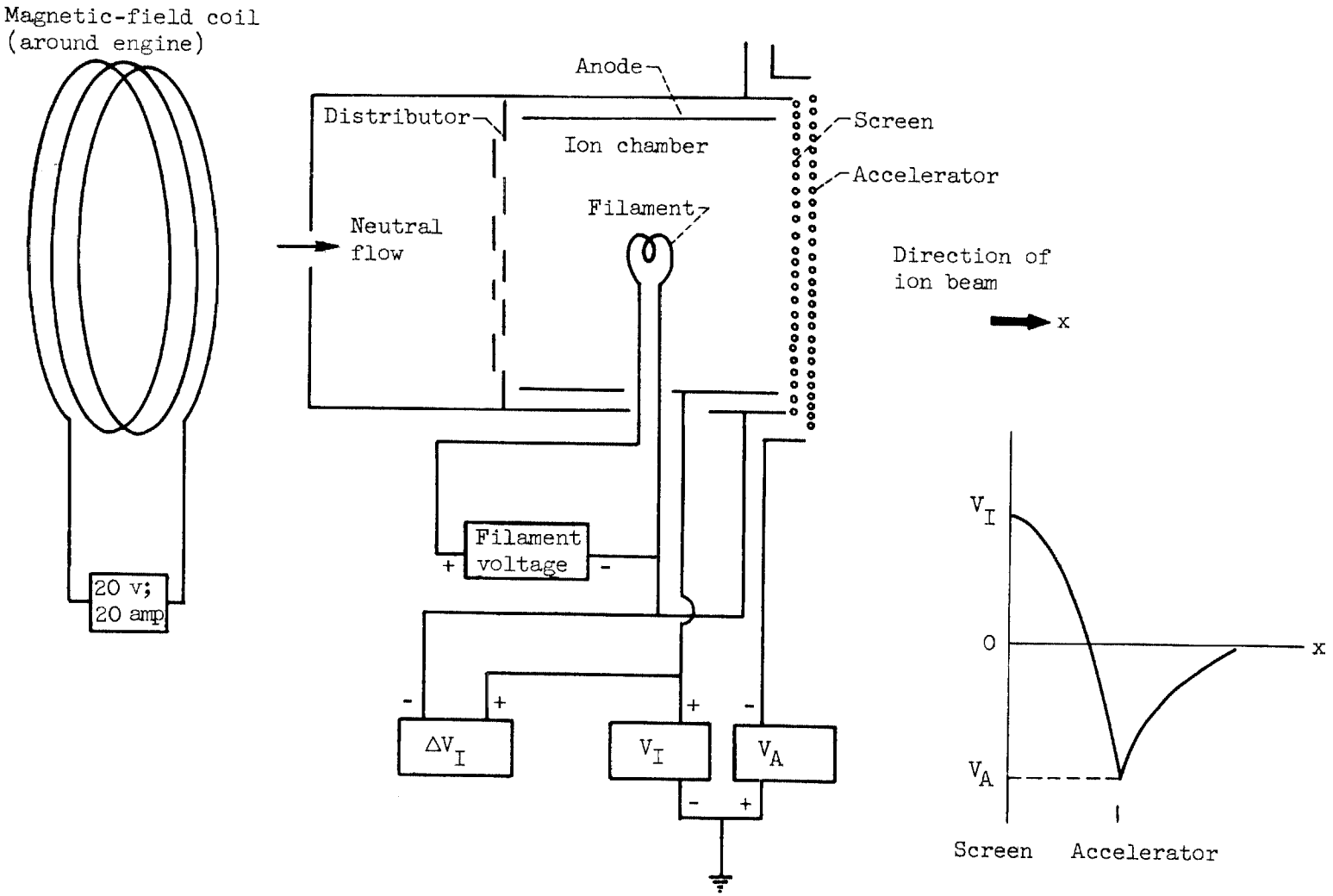

(b) Schematic diagram.

Figure 2. - Concluded. Electron-bombardment ion-rocket engine.

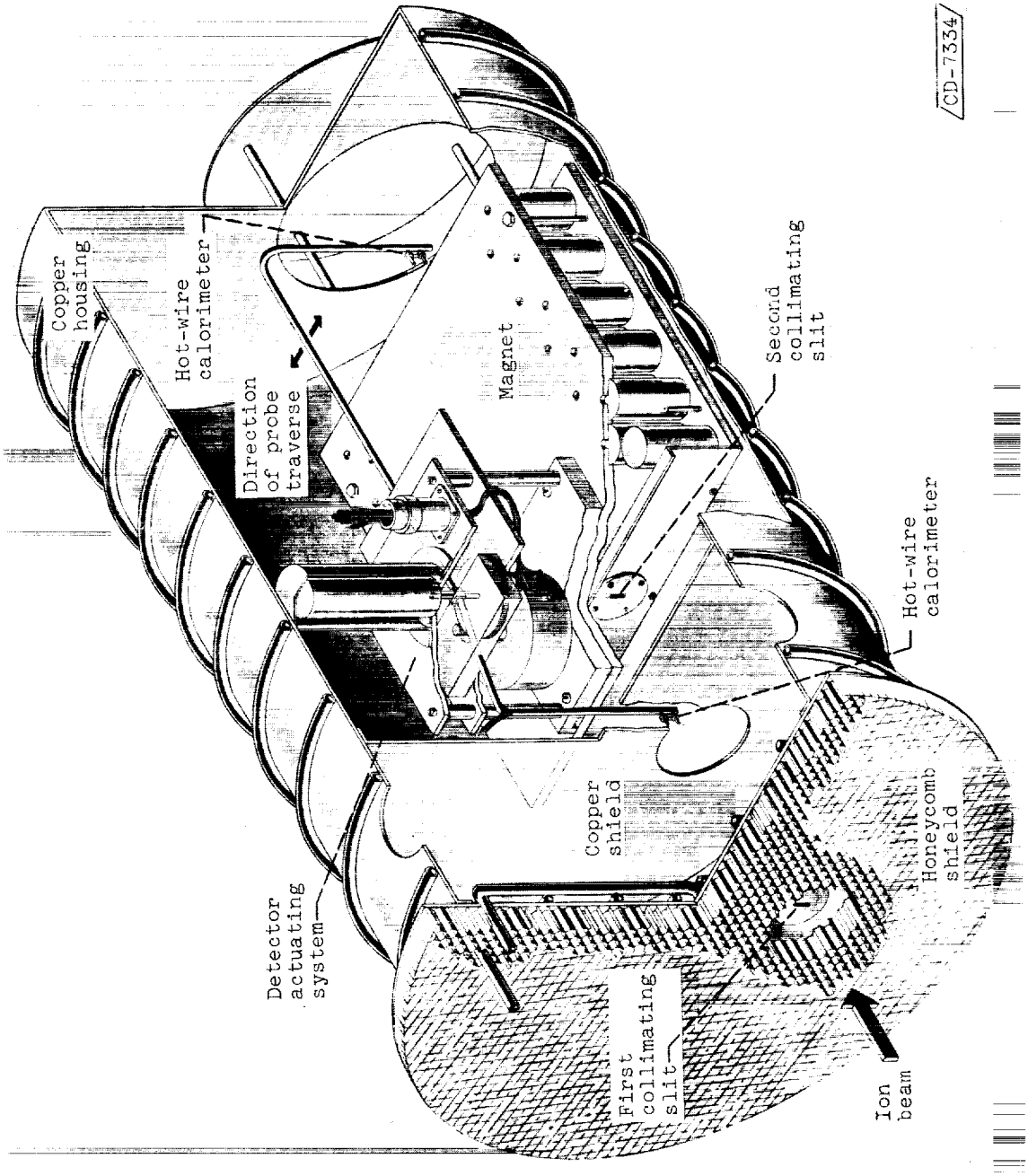

Figure 3. - Mass spectrometer.

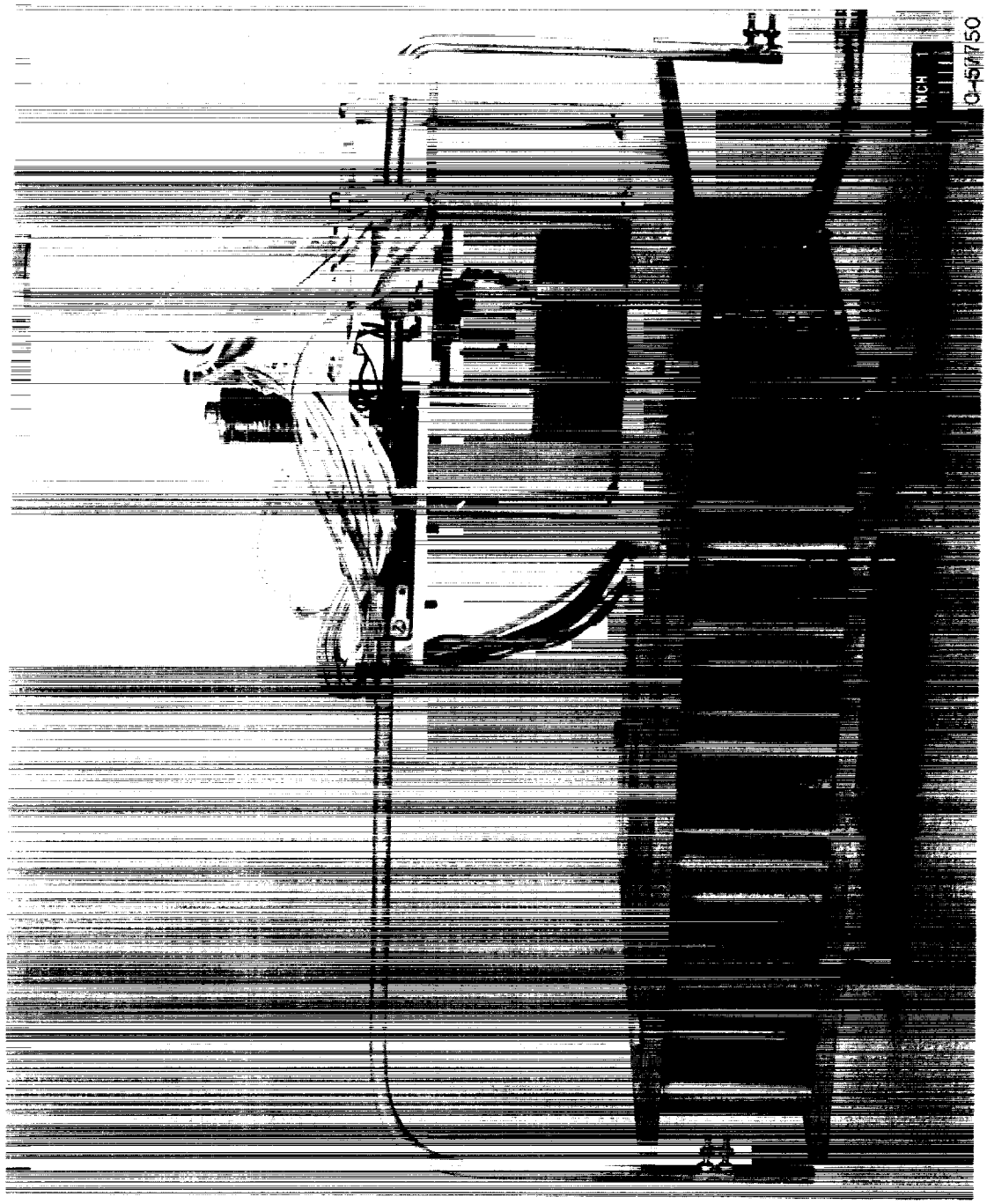

Figure 4. - Spectrometer magnet assembly and detector.

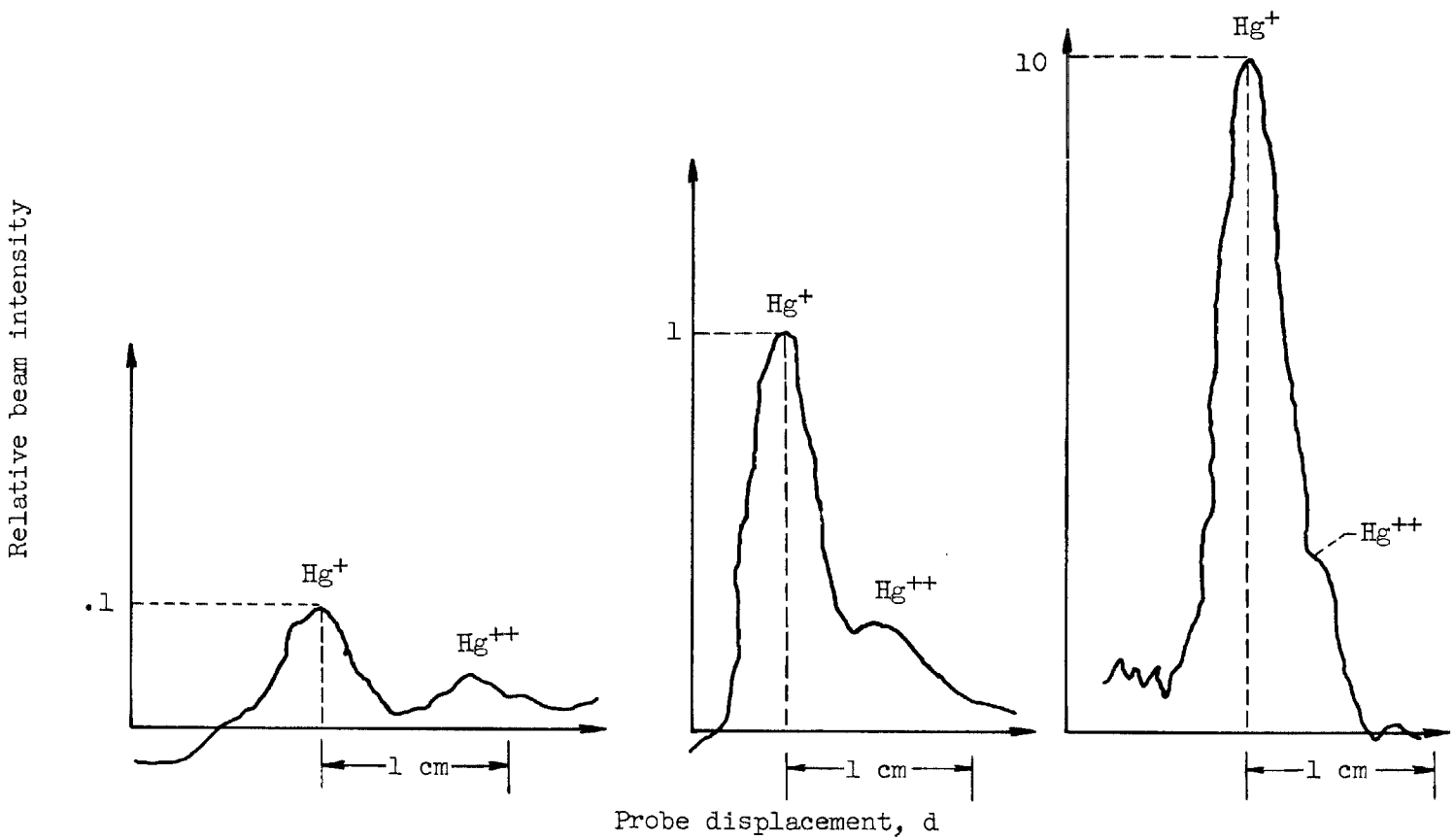

(a) Net accelerating voltage, 900 volts; ion-chamber potential difference, 100 volts.

(b) Net accelerating voltage, 2500 volts; ion-chamber potential difference, 60 volts.

(c) Net accelerating voltage, 4900 volts; ion-chamber potential difference, 100 volts.

Figure 5. - Characteristic recorder traces at different engine operating conditions.

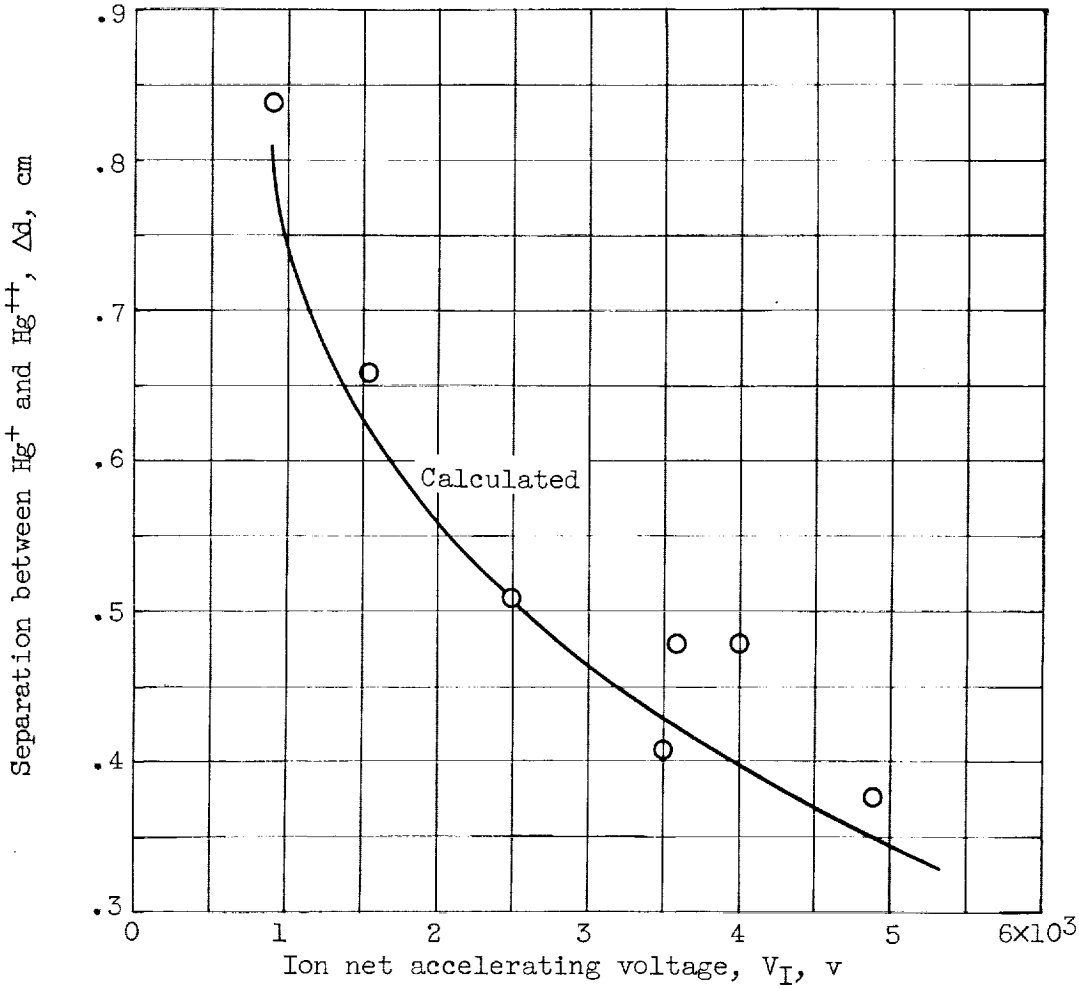

Figure 6. - Variation of separation between singly and doubly ionized mercury with ion net accelerating voltage in magnetic field of 400 gauss.

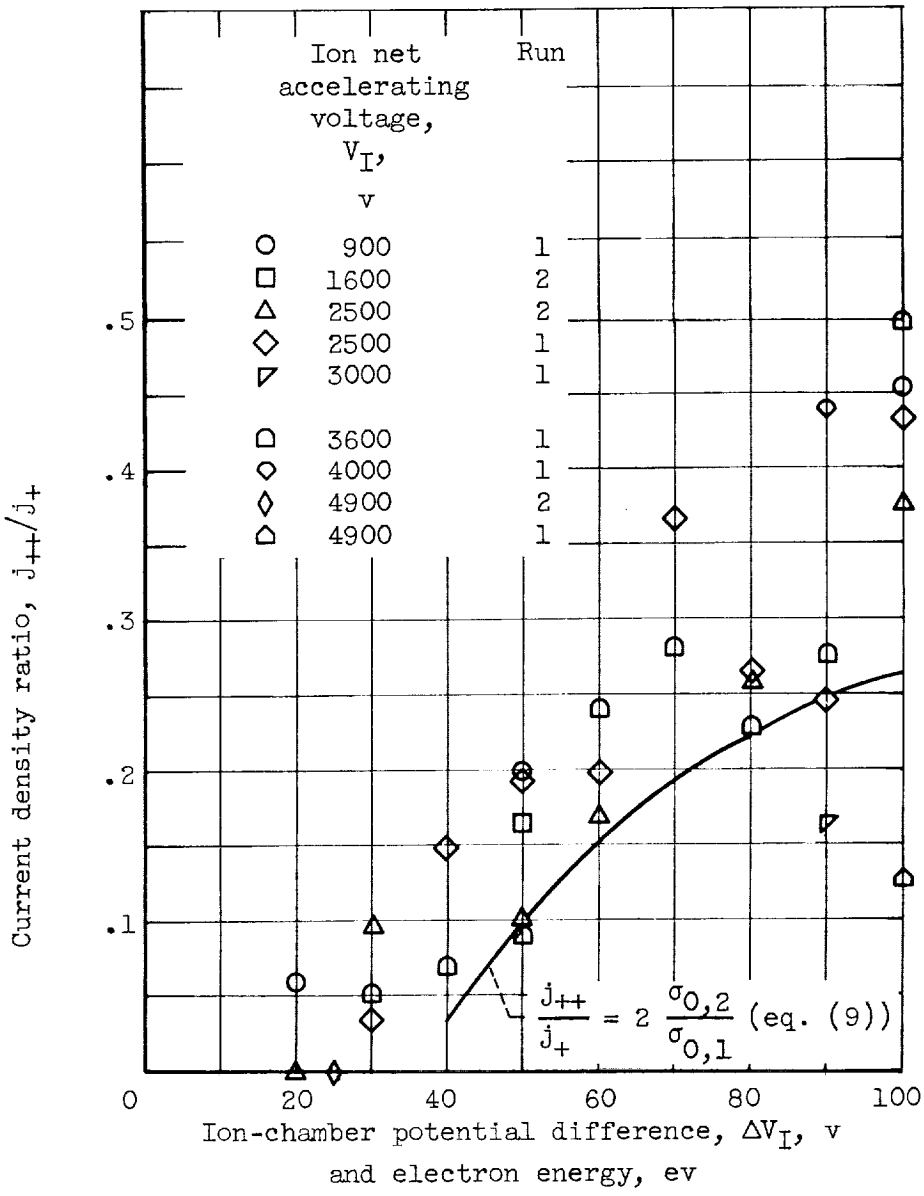

Figure 7. - Current density ratio as function of ion-chamber potential difference. Propellant utilization efficiency, 80 percent.

NASA TN D-1219
National Aeronautics and Space Administration.
COMPARATIVE MEASUREMENTS OF SINGLY AND DOUBLY IONIZED MERCURY PRODUCED BY ELECTRON-BOMBARDMENT ION ENGINE.
Nelson L. Milder. July 1962. 21p. OTS price, $0.75. (NASA TECHNICAL NOTE D-1219)

An ion-beam exhaust from an electron-bombardment ion engine was studied with a mass spectrometer. Ion-chamber potential differences were varied between 20 and 100 v for net accelerating voltages from 900 to 4900 v. Two ionic species corresponding to Hg^{+} and Hg^{++} were observed. The fraction of the total beam current due to Hg^{++} varied from approximately 0.05 at low chamber potential differences to over 0.3 at high potential differences.

I. Milder, Nelson L.
II. NASA TN D-1219

(Initial NASA distribution: 20, Fluid mechanics; 31, Physics, nuclear and particle; 41, Propulsion systems, electric.)

NASA

NASA TN D-1219
National Aeronautics and Space Administration.
COMPARATIVE MEASUREMENTS OF SINGLY AND DOUBLY IONIZED MERCURY PRODUCED BY ELECTRON-BOMBARDMENT ION ENGINE.
Nelson L. Milder. July 1962. 21p. OTS price, $0.75. (NASA TECHNICAL NOTE D-1219)

An ion-beam exhaust from an electron-bombardment ion engine was studied with a mass spectrometer. Ion-chamber potential differences were varied between 20 and 100 v for net accelerating voltages from 900 to 4900 v. Two ionic species corresponding to Hg^{+} and Hg^{++} were observed. The fraction of the total beam current due to Hg^{++} varied from approximately 0.05 at low chamber potential differences to over 0.3 at high potential differences.

I. Milder, Nelson L.
II. NASA TN D-1219

(Initial NASA distribution: 20, Fluid mechanics; 31, Physics, nuclear and particle; 41, Propulsion systems, electric.)

NASA

NASA TN D-1219
National Aeronautics and Space Administration.
COMPARATIVE MEASUREMENTS OF SINGLY AND DOUBLY IONIZED MERCURY PRODUCED BY ELECTRON-BOMBARDMENT ION ENGINE.
Nelson L. Milder. July 1962. 21p. OTS price, $0.75. (NASA TECHNICAL NOTE D-1219)

An ion-beam exhaust from an electron-bombardment ion engine was studied with a mass spectrometer. Ion-chamber potential differences were varied between 20 and 100 v for net accelerating voltages from 900 to 4900 v. Two ionic species corresponding to Hg^{+} and Hg^{++} were observed. The fraction of the total beam current due to Hg^{++} varied from approximately 0.05 at low chamber potential differences to over 0.3 at high potential differences.

I. Milder, Nelson L.
II. NASA TN D-1219

(Initial NASA distribution: 20, Fluid mechanics; 31, Physics, nuclear and particle; 41, Propulsion systems, electric.)

NASA

NASA TN D-1219
National Aeronautics and Space Administration.
COMPARATIVE MEASUREMENTS OF SINGLY AND DOUBLY IONIZED MERCURY PRODUCED BY ELECTRON-BOMBARDMENT ION ENGINE.
Nelson L. Milder. July 1962. 21p. OTS price, $0.75. (NASA TECHNICAL NOTE D-1219)

An ion-beam exhaust from an electron-bombardment ion engine was studied with a mass spectrometer. Ion-chamber potential differences were varied between 20 and 100 v for net accelerating voltages from 900 to 4900 v. Two ionic species corresponding to Hg^{+} and Hg^{++} were observed. The fraction of the total beam current due to Hg^{++} varied from approximately 0.05 at low chamber potential differences to over 0.3 at high potential differences.

I. Milder, Nelson L.
II. NASA TN D-1219

(Initial NASA distribution: 20, Fluid mechanics; 31, Physics, nuclear and particle; 41, Propulsion systems, electric.)

NASA